

## Plasma Heating due to Cyclic Diffusion across a Separatrix

F. Anderegg, M. Affolter, D. H. E. Dubin, and C. F. Driscoll

Physics Department 0319, University of California San Diego, La Jolla, California 92093, USA

 (Received 30 April 2018; published 6 September 2019)

We observe plasma heating due to collisional diffusion across a separatrix when a magnesium ion column in a Penning-Malmberg trap is cyclically pushed back and forth across a partial trapping barrier. The barrier is an externally applied axisymmetric “squeeze” potential, which creates a velocity separatrix between trapped and passing particles. Weak ion-ion collisions then cause separatrix crossings, leading to irreversible heating. The heating rate scales as the square root of the oscillation rate times the collision frequency and thus can be dominant for low-collisionality plasmas. The particle velocity distribution function is measured with coherent laser induced fluorescence and shows passing and trapped particles having an out-of-phase response to the forced plasma oscillations.

DOI: [10.1103/PhysRevLett.123.105002](https://doi.org/10.1103/PhysRevLett.123.105002)

Electric and magnetic field inhomogeneities in plasmas can create collisional boundary layers between trapped and passing particles. These boundary layers are predicted to enhance plasma transport [1,2], dissipate poloidal rotation [3], and damp waves [4,5]. Experiments, numerical simulations, and theories on tokamaks [6,7], stellarators [8,9], and pure electron plasmas [10–14] have shown increased transport and wave damping resulting from applied field inhomogeneities. However, prior experiments have not directly observed the signature  $\sqrt{\nu_c f_{sl}}$  scaling of these boundary layer analyses, where  $\nu_c$  is the collisionality and  $f_{sl}$  is the frequency at which the particles are cyclically pushed across the separatrix.

A heating rate proportional to  $\sqrt{\nu_c f_{sl}}$  is similar to the viscous heating of a sheared fluid caused by an oscillating plate [15,16]. Here, oscillating untrapped plasma takes the place of the plate, transferring energy and momentum diffusively into the trapped plasma through a boundary layer of width proportional to  $\sqrt{\nu_c/f_{sl}}$ , as in the classic fluid problem.

In this Letter, we present quantitative measurements of the particle dynamics in the presence of a velocity separatrix and of the resulting plasma heating induced by collisional diffusion across this separatrix. Trapped and passing particle populations are created by applying a cylindrically symmetric electrostatic squeeze near the middle of a pure ion plasma column. When the plasma is cyclically pushed through this potential barrier, the trapped and passing particles experience different dynamics, forming a collisional boundary layer. The particle dynamics are directly measured using a coherent laser induced fluorescence technique, and the trapped (passing) particles are observed to move in (out of) phase with the applied forcing, in quantitative agreement with a recent collisionless adiabatic invariant analysis [17].

Ion-ion collisions cause velocity diffusion and separatrix crossings, which leads to irreversible heating scaling as  $\dot{T}/T \propto \sqrt{\nu_c f_{sl}} (e\phi_s)^2 \delta L^2$ , where  $\delta L$  is the amplitude of the forced oscillation through the separatrix potential  $e\phi_s$  created by the externally applied  $V_{sqz}$ . This heating is in quantitative agreement with recent theory [17]. The cyclic nature of the oscillation, effectively *restarts* the diffusion process at each cycle, resulting in “cyclic diffusion” of particles across the separatrix.

These experiments for the first time confirm the signature  $\sqrt{\nu_c f_{sl}}$  scaling of the collisional separatrix heating, by changing the rate  $f_{sl}$  at which the plasma is oscillated through the squeeze and by changing ion-ion collisionality  $\nu_c$  over a range of  $100\times$  in  $\nu_c f_{sl}$ .

A Penning-Malmberg trap with a wall radius  $R_W = 2.86$  cm is used to confine un-neutralized magnesium ions in a magnetic field of  $B = 3$  T [18], as shown in Fig. 1.

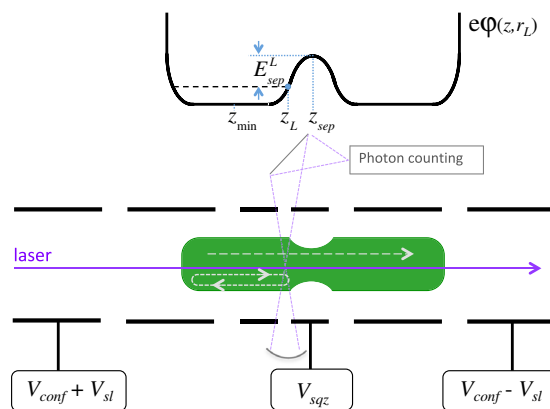


FIG. 1. Pure ion plasma in a Penning-Malmberg trap forced through squeeze with oscillating voltage  $V_{sl}$ . The figure shows the plasma pushed to the right, defined as phase  $0^\circ$ . The top curve sketches potential along the magnetic field at the laser radial position.

These traps can contain the same charged particles in steady state for weeks [19], by using weak “rotating-wall” electric potentials [20]. Using laser induced fluorescence diagnostics on the ground state of  $\text{Mg}^+$  ( $\lambda \simeq 280$  nm), the plasma radial density profile  $n(r, z_L)$  and temperature  $T(r, z_L)$  are measured at the laser location  $z_L$ , and the 2D density  $n(r, z)$  is then calculated using a Boltzmann-Poisson solver [21]. A typical plasma, axially confined with  $V_{\text{conf}} = 100$  V, has a length  $L_p \simeq 11$  cm and a radially uniform density  $n_0 \simeq 2 \times 10^7 \text{ cm}^{-3}$  out to  $R_p \simeq 0.5$  cm, resulting in an almost rigid  $E \times B$  plasma rotation at a frequency  $f_{E \times B} \simeq 10$  kHz. The ions cool toward 0.04 eV from collision with neutral  $\text{H}_2$  at pressure  $P \simeq 10^{-8}$  torr and applied weak cyclotron heating on the  $^{24}\text{Mg}^+$  ions controls the plasma temperature over the range  $0.04 < T < 1$  eV. Initial radial temperature profiles are uniform within 10% inside most of the plasma and typically 25% warmer on the edge (see, e.g., Ref. [22]). The temperature is presumed to be uniform in  $z$ .

For these experiments, a velocity separatrix is created by applying a squeeze potential  $V_{\text{sqz}}$  to an annular electrode as shown in Fig. 1. The cyclic axial plasma flow (sloshing) is formed by adding nominally sinusoidal voltages  $\pm V_{\text{sl}} \cos(2\pi f_{\text{sl}} t)$  to the end confinement voltages  $V_{\text{conf}}$ , with the + (−) referring to the left (right) end. Typically, the slosh frequency  $f_{\text{sl}} = 500$  Hz, and the slosh amplitude  $V_{\text{sl}} \simeq 50$  V<sub>p</sub> effectively displaces each end a distance  $\pm \delta L \approx 0.5$  cm.

To test recent theory [17], these experiments are performed in the “superbanana” regime defined by  $\nu_c \ll 2\pi f_{\text{sl}} \ll 2\pi f_b$  [8,17]. Here the axial bounce frequency is  $f_b = \bar{v}/2L_p \simeq 10 \text{ kHz} (10 \text{ cm}/L_p)(T/1 \text{ eV})^{1/2}$  with  $\bar{v} = 2 \times 10^5 (T/1 \text{ eV})^{1/2} \text{ cm/s}$ . The classical ion-ion collision rate given by  $\nu_c \equiv \frac{4}{3} \sqrt{\pi} n \bar{v} b^2 \ln(r_c/b) \simeq 1.0 \text{ s}^{-1} (n/10^7 \text{ cm}^{-3})(T/1 \text{ eV})^{-3/2}$ . In this temperature regime, bulk viscous heating (scaling as  $\nu_c/f_{\text{sl}}$ ) is substantially weaker [23] than the separatrix heating. Also  $f_{\text{sl}} < f_b$ , so that the ( $\nu_c$ -independent) heating due to excitation of bounce resonances is minimized [23].

The particle dynamics is measured using a coherent laser induced fluorescence (LIF) technique [24], which measures the parallel velocity distribution function  $F(v, z_L)$  coherent with the phase  $\theta(t)$  of the forced plasma sloshing. Reference [18] describes the ground state  $\text{Mg}^+$  LIF scheme at 280 nm, while Ref. [24] describes the coherent LIF technique. The laser wavelength is set to be resonant with a  $\text{Mg}^+$  ion moving at velocity  $v$ . The plasma is then sinusoidally forced back and forth through the separatrix  $\varphi_s$  for 500 ms (250 cycles at 500 Hz) and the time of arrival of each fluorescent photon is recorded along with the phase of the slosh. The plasma is then allowed to reequilibrate for 10 s, and the process is repeated for 100 different laser wavelengths, encompassing the entire particle velocity distribution.

Postprocessing of the data assigns each photon from each wavelength (velocity) into 16 phase bins  $\theta_j = j2\pi/16$

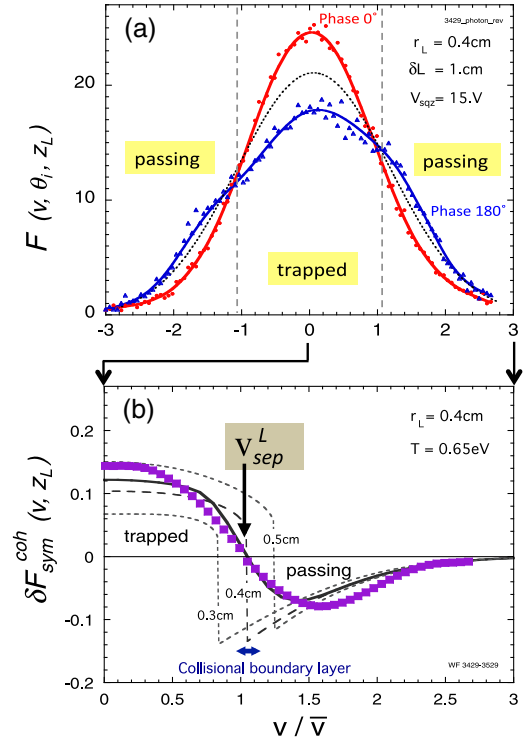


FIG. 2. (a) Measured velocity distribution shown for phase  $0^\circ$  (plasma pushed to the right) and phase  $180^\circ$  (plasma pushed to the left). (b) Symmetric coherent response of the velocity distribution. Measurements are shown with squares, and the solid line is the theory prediction averaged over the 0.1 cm radius of the laser beam. Horizontal axes are normalized particle velocity.

corresponding to the slosh phase at the photon time, and the entire phase-coherent distribution is reconstructed as  $F(v, \theta_j, z_L)$ . Because of the finite size of the laser beam and viewing volume, these measurements are convolved over a 0.2 cm diameter, 0.3 cm long cylinder centered at  $z_L$ . The beam diameter was selected to optimize the signal to noise and minimize nonlinear distortion of the distribution function.

Figure 2(a) shows the coherent  $F(v, \theta_j, z_L)$ , obtained during 125 slosh cycles, at two phases corresponding to the right (phase  $0^\circ$ ) and left (phase  $180^\circ$ ) slosh extremes. For phase  $0^\circ$  (red dots), the plasma is being forced to the right as shown in Fig. 1. Therefore, the *trapped* particles at the laser location  $z_L$  are compressed, giving a larger density at low velocity. In contrast, the density of *passing* particles at  $z_L$  decreases to equalize the potential along a given field line. For phase  $180^\circ$  (blue triangles), the plasma is forced to the left, and the density changes are reversed. The dotted line of Fig. 2(a) is the Maxwellian distribution  $F_M(v)$  before sloshing, and the two vertical gray dashed lines indicate the minimum particle velocity  $v_{\text{sep}}^L$  at the laser location required to cross the separatrix. The asymmetries in the measured  $F(v)$  are due to small fractions of magnesium isotope 25 and 26.

We also observe that the entire distribution of particles is sloshing at a low velocity. For the data presented in Fig. 2(a),  $v_{sl} \simeq 5000$  cm/s  $\simeq 0.03\bar{v}$  is measurable, but too small to be visible on this plot. Assuming a forced sinusoidal oscillation of the plasma, the in phase [25] coherent change of the distribution is

$$\delta F^{\text{coh}}(v) \equiv \sum_{j=0}^{15} F(v, \theta_j) \times \cos \theta_j. \quad (1)$$

Changes in the plasma density and temperature appear in the  $v$ -symmetric response given by

$$\delta F_{\text{sym}}^{\text{coh}}(v) \equiv \frac{1}{2F_M(0)} [\delta F^{\text{coh}}(v) + \delta F^{\text{coh}}(-v)], \quad (2)$$

where  $F_M$  is the initial Maxwellian distribution. The analogous  $v$ -antisymmetric response yields the fluid velocity of the particles.

The symmetric coherent response  $\delta F_{\text{sym}}^{\text{coh}}(v, z_L)$  is plotted in Fig. 2(b). The horizontal axis is the measured particle velocity at  $z_L$ , normalized to the initial thermal velocity  $\bar{v} = 1.6 \times 10^5$  cm/s from temperature  $T = 0.65$  eV. Each symbol corresponds to measurements performed at two wavelengths of the laser, corresponding to  $\pm v$ . The collision rate is  $\nu_c = 3.8$  s $^{-1}$ , so a thermal ion experiences about two collisions during the 250 slosh cycles. The symmetric response  $\delta F_{\text{sym}}^{\text{coh}}(v)$  clearly shows that the trapped particles ( $v < 1.05\bar{v}$ , at this measurement radius,  $r_L = 0.4$  cm) are in-phase with the forcing, whereas the passing particles ( $v > 1.05\bar{v}$ ) are out of phase. At phase 0° (sloshed right), the left-trapped density increases, while the passing particle in the left density decreases. The velocity where  $\delta F_{\text{sym}}^{\text{coh}}(v) = 0$  is the measured separatrix velocity  $v_{\text{sep}}^L$  at the laser location.

The curves of Fig. 2(b) are the predicted  $\delta F_{\text{sym}}^{\text{coh}}(v, z_L, r_L)$  from the theory of Ref. [17]. This theory first evaluates the collisionless adiabatic response to the  $\cos(2\pi f_{sl}t)$  oscillation in the external potential. Assuming the variations are small, so that linear theory can be applied, the perturbed distribution is

$$\delta F(z, v_z, r, t) = -\cos(2\pi f_{sl}t) \frac{e\delta\varphi(z, r) - e\langle\delta\varphi\rangle(r, E)}{T}. \quad (3)$$

Here  $E(z, v_z, r) = e\varphi + \frac{1}{2}mv_z^2$  is the energy of a particle,  $\delta\varphi(z, r) \cos(2\pi f_{sl}t)$  is the perturbed electrostatic potential, and the angle brackets indicate a ‘‘bounce average’’ over a collisionless particle orbit. The particle dynamics is at fixed  $r$ , but the potentials  $\varphi(z, r)$  and  $\delta\varphi(r, z)$  are determined by a self-consistent solution of Poisson’s equation with the wall boundary conditions. Thus, the separatrix energy  $E_{\text{sep}}(z, r)$  depends strongly on  $r$ , and passing particles will ‘‘shield’’ the potential from trapped particles at other radii.

The long dashed line of Fig. 2(b) is the collisionless theory prediction of  $\delta F_{\text{sym}}^{\text{coh}}(v)$  for  $r = 0.4$  cm, showing a sharp discontinuity at the separatrix. The discontinuity is due to the bounce average of  $\delta\varphi$  being different for trapped and passing particles. The short dashed lines are the theory predictions for  $r = 0.3$  and  $0.5$  cm corresponding to the edges of the laser beam. The solid line is the prediction of  $\delta F_{\text{sym}}^{\text{coh}}(v)$  averaged over the laser beam, predicting a smooth measured distribution. Data with an increased beam size (not shown) corroborate the effect of spatial averaging.

The particle kinetic energy required to pass through the squeeze is a function of  $z$  position and radius in the plasma, and we determine  $E_{\text{sep}}^L(z_L, r_L) \equiv \frac{1}{2}m[v_{\text{sep}}^L(z_L, r_L)]^2$  by detecting the change of sign in the symmetric response of  $\delta F_{\text{sym}}^{\text{coh}}(v)$  occurring at  $v_{\text{sep}}^L$ , as shown in Fig. 2(b). Note that the LIF measures the kinetic energy of particles only at  $z = z_L$ , so particles with energy less than  $\varphi(z_L, r)$  are not detected, since they do not have enough energy to reach the diagnostic location. On axis  $r = 0$ , at  $z_{\text{min}}$ , the potential with respect to the trap wall is  $e\varphi(z_{\text{min}}, r = 0) = 14.89$  eV, at the laser location is  $e\varphi(z_L, r = 0) = 14.98$  eV, and  $e\varphi(z_{\text{sep}}, r = 0) = 15.11$  eV; this gives a separatrix energy relative to the laser position of  $E_{\text{sep}}^L \equiv e\varphi(z_{\text{sep}}, r = 0) - e\varphi(z_L, r = 0) = 0.13$  eV. These potentials are calculated from the Poisson-Boltzmann equilibrium [21]. The estimated absolute accuracy is  $\pm 0.1$  V due to uncertainty in the total number of ions, and the estimated relative accuracy at various locations is  $\pm 0.02$  V.

Figure 3(a) compares the LIF-determined  $E_{\text{sep}}^L$  (squares) to that calculated from the Boltzmann-Poisson equilibrium  $e\varphi(z, r)$  (open circles), as a function of radius. This corroborates the interpretation of  $v_{\text{sep}}^L$  on Fig. 2(b). Figure 3(a) shows that  $E_{\text{sep}}^L$  is reduced by Debye shielding in the center. Measurements at all seven radial locations are performed on the same plasma, but due to repeated sloshing through the squeeze potential some particles on the outside edge of the plasma are lost. The plasma radius evolves from 0.64 to 0.57 cm over the course of the measurement. The data are collected at ‘‘interlaced’’ radii to avoid systematic drift. The theory predictions of Fig. 3 are calculated at each specific radius for the measured experimental conditions. The lines on Fig. 3 are merely to guide the eye.

Integrating  $\delta F_{\text{sym}}^{\text{coh}}(v, r)$  gives the density perturbation  $\delta n^{\text{coh}}(r)$  plotted versus radius in Fig. 3(b) (triangles), with the theory prediction from integrating Eq. (2) (open circles). At large radii most particles are trapped and  $\delta n^{\text{coh}} > 0$ , because the trapped density increases as the trapped plasma is compressed. In contrast, at small radii  $\delta n^{\text{coh}} < 0$ , because most particles are passing and can move to shield out trapped particle density charges.

The second half of this Letter focuses on the plasma heating caused by collisions acting on this particle dynamics. As the trapped particles are compressed or expanded

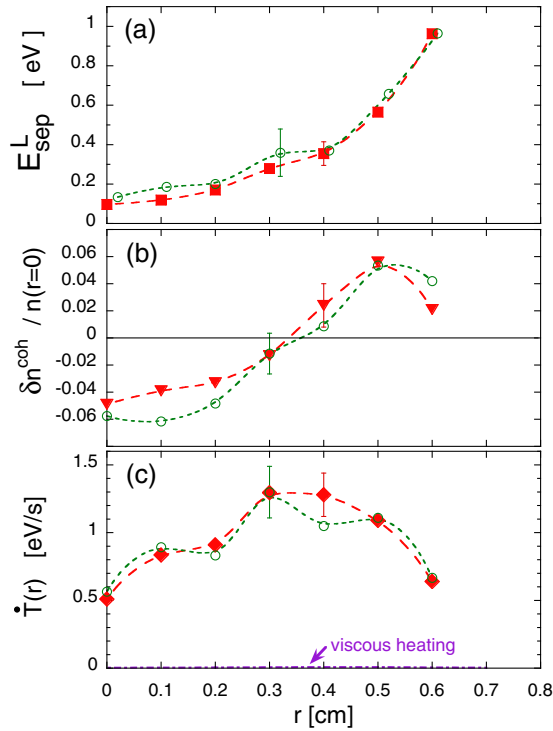


FIG. 3. Radial profile at “laser location”  $z_L$  of (a) Kinetic particle energy required to cross separatrix, (b) coherent density perturbation, and (c) heating rate  $\dot{T}$  plotted against radius. Solid symbols are experimental measurement and open symbols are theory predictions.

by the slosh, they undergo an adiabatic change in temperature  $\delta T = \pm 2T(\delta L/L)^2$  every period of the slosh oscillation, where the  $\pm$  indicates that  $\delta T$  reverses sign across the separatrix. Collisions then cause particles with energy near the separatrix energy  $e\varphi_s$  to make a trapped or passing transition before the slosh perturbation reverses; this defines a collisional boundary layer of energy width  $\Delta E = \sqrt{Te\varphi_s\nu_c/(2\pi f_{sl})}$  around the separatrix. For the case presented in Fig. 2(b), the width of the boundary layer is small with  $\Delta E = 0.02$  eV.

Collisions make the adiabatic heating of the trapped particles irreversible, which leads to plasma heating scaling as  $f_{sl}(e\varphi_s)^2(\delta L/L)^2\alpha_{BL}$ , where  $\alpha_{BL}$  is the fraction of particles in the boundary layer. For a Maxwellian distribution,  $\alpha_{BL} \sim (\Delta E/\sqrt{Te\varphi_s})\exp(-e\varphi_s/T)$ , so the heating rate is

$$\frac{\dot{T}}{T} \sim \sqrt{\nu_c f_{sl}} (e\varphi_s/T)^2 (\delta L/L)^2 \exp(-e\varphi_s/T). \quad (4)$$

The exact expression for the heating rate can be found in Eq. (51) of Ref. [17] and was used to calculate the open circles of Fig. 3(c) for each radius. Theory and experiment are in quantitative agreement at each radius and show that the maximum heating occurs where about half the particles

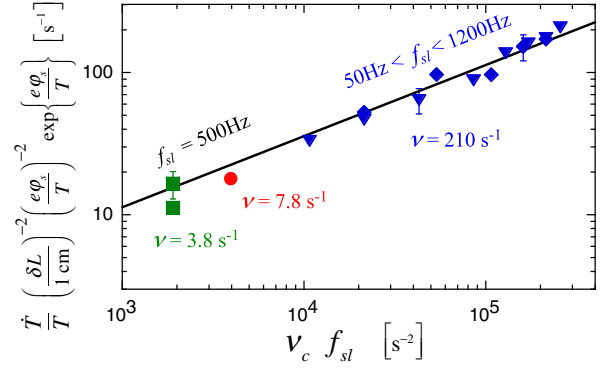


FIG. 4. Normalized heating rate  $\dot{T}/T$  plotted versus collision rate times sloshing frequency, showing heating rate proportional to  $\sqrt{\nu_c f_{sl}}$ .

are trapped. Note that theory generally describes the heating per cycle scaling as  $\sqrt{\nu_c/f_{sl}}$ . Experimentally, we measure the heating rate (per unit of time) that scales as  $f_{sl}\sqrt{\nu_c/f_{sl}} = \sqrt{\nu_c f_{sl}}$ . The temperature is measured before and after the multicycle slosh through a squeeze at which times the distributions are close to Maxwellian.

We vary  $V_{sqz}$  to change the separatrix energy  $e\varphi_s$ . In these experiments, we observe a heating rate with the  $(e\varphi_s)^2 \exp(-e\varphi_s/T) \delta L^2$  scaling of Eq. (4) over the range  $3 < V_{sqz} < 15$  V and  $0.35 < \delta L < 1.8$  cm.

We also for the first time observe the  $\sqrt{\nu_c f_{sl}}$  heating rate characteristic of boundary layer analysis. Figure 4 displays the measured heating rate for a wide range of plasma parameters, confirming the  $\sqrt{\nu_c f_{sl}}$  scaling over a factor of 100 in  $\nu_c f_{sl}$ . Here, the four different symbols represent  $\nu_c$  and  $f_{sl}$  values as shown. The heating rate  $\dot{T}/T$  is scaled as expected theoretically for the  $(\delta L/L)^2$  amplitude of the displacement, for the  $(e\varphi_s/T)^2$  ratio of potential to thermal energies, and for the  $\exp(-e\varphi_s/T)$  dependence of the number of particles at the separatrix energy. The squares are the normalized heating rate for the low-collisionality plasma ( $\nu_c \simeq 3.8$  s $^{-1}$ ) of Figs. 2 and 3 at  $r_L = 0.3$  and 0.4 cm. The dot is from a plasma with  $\nu_c = 7.8$  s $^{-1}$ . The blue symbols are for  $\nu_c \simeq 210$  s $^{-1}$ , the triangles are for  $\delta L = 1$  cm, diamonds are for  $\delta L = 1.8$  cm, and sloshing frequencies are  $50 < f_{sl} < 1200$  Hz. The symbols of Fig. 4 cover a range of 55 in collisionality  $\nu_c$  and 24 in frequency  $f_{sl}$ . The solid line is the heating rate predicted by theory with no adjustable parameter from Eq. (51) of Ref. [17].

To control the temperature and therefore the ion-ion collision rate, we typically keep the hydrogen pressure fixed and change the amount of cyclotron heating. We have used other combinations of hydrogen pressure and cyclotron heating to obtain the same temperature. The heating due to separatrix crossings is caused by ion-ion collisions, and we observe the same separatrix heating rate for other combinations of pressure and cyclotron heating. The (slower) cooling collisions with neutral H $_2$  molecules

are not essential to the observed heating due to separatrix crossing.

Experimentally, it is worth noting that oscillating the plasma in the absence of a separatrix produces negligible heating. Furthermore, applying a negative squeeze voltage does not produce separatrix heating, since it does not create a separatrix between separate trapped populations. For example, applying  $V_{\text{sqz}} = -15$  V on a plasma similar to the one used in Figs. 2 and 3 results in a negligible heating rate  $\dot{T} \simeq 0.02$  eV/s at  $r_L = 0.4$  cm.

Other mechanisms can also heat the plasma, albeit at a much slower rate when  $\nu_c \ll 2\pi f_{\text{sl}}$ . For instance, cyclic plasma compressions and expansions causes bulk viscous heating of order  $\nu_c T (\delta L/L)^2$  [23], and our “slosh” procedure also compress and expands the trapped particles. For the plasma data of Fig. 3, this bulk viscous heating is maximum at  $r = 0.42$  cm, where  $\dot{T}_{\text{vis}} = 0.009$  eV/s about 100 times smaller than the heating attributed to separatrix dissipation, as shown by the dotted line at the bottom of the graph. For the large collisionality data  $\nu_c = 210$  s<sup>-1</sup> of Fig. 4, bulk viscous heating is about 15 times smaller than the heating attributed to separatrix dissipation.

To summarize, we have used external electrodes to create a controlled velocity space separatrix and have forced the plasma to oscillate through it at frequencies in the superbanana regime  $\nu_c \ll 2\pi f_{\text{sl}} \ll 2\pi f_b$ . We experimentally identify passing and trapped particles and have observed directly the coherent particle response in quantitative agreement with newly developed theory. Furthermore, these experiments for the first time confirm plasma heating scaling as  $\sqrt{\nu_c f_{\text{sl}}}$ , in quantitative agreement with superbanana heating due to particle diffusively crossing an energy separatrix. This heating mechanism is relatively large for low-collisionality plasma and can be significant for fusion plasma.

This work was supported by Department of Energy Award No. DE-SC0018236, National Science Foundation Grant No. PHY-1805764, and AFOSR Grant No. FA9550-19-1-0099. M. A. was partially supported by the DOE FES Postdoctoral Research Program administered by ORISE for the DOE. ORISE is managed by ORAU under DOE Award No. DE-SC0014664.

---

[1] A. A. Galeev, R. Z. Sagdeev, H. P. Furth, and M. N. Rosenbluth, *Phys. Rev. Lett.* **22**, 511 (1969).

- [2] K. C. Shaing, P. Cahyna, M. Becoulet, J.-K. Park, S. A. Sabbagh, and M. S. Chu, *Phys. Plasmas* **15**, 082506 (2008).
- [3] R. C. Morris, M. G. Haines, and R. J. Hastie, *Phys. Plasmas* **3**, 4513 (1996).
- [4] T. J. Hilsabeck, A. A. Kabantsev, C. F. Driscoll, and T. M. O’Neil, *Phys. Rev. Lett.* **90**, 245002 (2003).
- [5] M. N. Rosenbluth, D. W. Ross, and D. P. Kostomarov, *Nucl. Fusion* **12**, 3 (1972).
- [6] W. Zhu, S. A. Sabbagh, R. E. Bell, J. M. Bialek, M. G. Bell, B. P. LeBlanc, S. M. Kaye, F. M. Levinton, J. E. Menard, K. C. Shaing, A. C. Sontag, and H. Yuh, *Phys. Rev. Lett.* **96**, 225002 (2006).
- [7] B. LaBombard, M. V. Umansky, R. L. Boivin, J. A. Goetz, J. Hughes, B. Lipschultz, D. Mossessian, C. S. Pitcher, J. L. Terry, and A. Group, *Nucl. Fusion* **40**, 2041 (2000).
- [8] H. Mynick, *Phys. Plasmas* **13**, 058102 (2006).
- [9] J. M. Faustin, W. A. Copper, J. P. Graves, D. Pfefferle, and J. Geiger, *Nucl. Fusion* **56**, 092006 (2016).
- [10] A. A. Kabantsev and C. F. Driscoll, *Phys. Rev. Lett.* **97**, 095001 (2006).
- [11] A. A. Kabantsev, D. H. E. Dubin, C. F. Driscoll, and Y. A. Tsidulko, *Phys. Rev. Lett.* **105**, 205001 (2010).
- [12] A. A. Kabantsev and C. F. Driscoll, *Phys. Rev. Lett.* **112**, 055003 (2014).
- [13] C. F. Driscoll, A. A. Kabantsev, D. H. E. Dubin, and Y. A. Tsidulko, *AIP Conf. Proc.* **1521**, 15 (2013).
- [14] J. Fajans, *Phys. Plasmas* **10**, 1209 (2003).
- [15] H. Lamb, *Hydrodynamics*, 6th ed. (Cambridge University Press, Cambridge, England, 1932).
- [16] G. K. Batchelor, *An Introduction to Fluid Dynamics* (Cambridge University Press, Cambridge, England, 1967).
- [17] D. H. E. Dubin, *Phys. Plasmas* **24**, 112120 (2017).
- [18] F. Anderegg, X.-P. Huang, E. Sarid, and C. F. Driscoll, *Rev. Sci. Instrum.* **68**, 2367 (1997).
- [19] D. H. E. Dubin and T. M. O’Neil, *Rev. Mod. Phys.* **71**, 87 (1999); T. M. O’Neil, *Phys. Today* **52**, No. 2, 24 (1999).
- [20] X.-P. Huang, F. Anderegg, E. M. Hollmann, C. F. Driscoll, and T. M. O’Neil, *Phys. Rev. Lett.* **78**, 875 (1997); E. M. Hollmann, F. Anderegg, and C. F. Driscoll, *Phys. Plasmas* **7**, 2776 (2000).
- [21] E. H. Chao, R. C. Davidson, S. F. Paul, and K. S. Fine, *AIP Conf. Proc.* **498**, 461 (1999).
- [22] F. Anderegg, X.-P. Huang, E. M. Hollmann, C. F. Driscoll, T. M. O’Neil, and D. H. E. Dubin, *Phys. Plasmas* **4**, 1552 (1997).
- [23] B. P. Cluggish, J. R. Danielson, and C. F. Driscoll, *Phys. Rev. Lett.* **81**, 353 (1998).
- [24] F. Anderegg, C. F. Driscoll, D. H. E. Dubin, and T. M. O’Neil, *Phys. Rev. Lett.* **102**, 095001 (2009).
- [25] A small 90° out-of-phase component is also observed but the signal is too noisy to be useful. That is, we are ignoring dissipation in this coherent description.